# Acoustic characteristics of damped metamaterial plate with parallel attached resonators

T. WANG[1,2], M. P. SHENG[1], Z. W. GUO[1], Q. H. QIN[2]

[1] *School of Marine Science and Technology*
*Northwestern Polytechnical University*
*Xi'an, Shaanxi, P.R. China 710072*

[2] *College of Engineering and Computer Science*
*the Australian National University*
*Acton, ACT, Australia 2601*
*e-mail: qinghua.qin@anu.edu.au*

AN ACOUSTIC METAMATERIAL CONSISTING of a homogeneous damped plate with parallel attached resonators is presented. Theoretical analysis shows that the metamaterial plate can generate multiple resonant-type band gaps and the lower-bound frequency of each band gap coincides with the resonance frequencies of the resonators. The parallel arrangement of resonators, compared with the metamaterial plate with resonators attached in series reported by PENG *et al.* (2015), results in a wider second band gap with a lower edge, while the first band gap is almost the same, creating therefore an easier combination of the multiple band gaps into a wider one. It is noted that damping has a significant influence on the band gaps and the effective mass density (especially for the damping of resonators). Specifically, it can be concluded that damping cannot be neglected in practical engineering applications, damping in the material of the host plate can smooth and lower the responses in the whole frequency range, especially in the higher frequency range, and a high level of damping of resonators deactivates the effect of band gaps. Such weak/damped resonators actualise the metamaterial damping poorly, and rather tend only to contribute to the overall damping such as the damping of the host plate.

**Key words:** acoustic metamaterial plate, damping effect, negative mass density, flexural wave propagation.

## 1. Introduction

AN ACOUSTIC METAMATERIAL is an artificial periodic structure having special properties such as effective negative mass density [1–3], effective negative Young's modulus [4–6] and negative refraction index [7], which cannot be observed in nature when a structure is treated as a homogeneous medium. The significance of acoustic metamaterials for practical applications lies in their confinement of elastic wave propagation. Frequency ranges where waves can propagate through the acoustic metamaterial are called pass bands, while frequency ranges within

which waves are completely blocked are known as band gaps. Researchers have recently attempted to obtain multiple broad band gaps by constructing different acoustic metamaterial structures and investigating their absorption of elastic waves and suppression of structural vibration. Early studies in this field focused on one-dimensional lattice [8–13] and were concerned with the constraints of longitudinal wave propagation only. In engineering applications, however, flexural waves propagate predominantly in classical structures and radiate energy to the surroundings, thus threatening the safety of the structure, and deleteriously influencing the accuracy of apparatus. Thus, structure design is vital for controlling the behaviour of flexural wave within continuum structures [14]. Several studies of flexural wave propagation in beams of acoustic metamaterial have been reported. YU et al. [15–17] attached local resonant structures to different beams such as Timoshenko and Euler–Bernoulli beams, to generate a flexural band gap through which flexural waves could not pass. CHEN et al. [18–20] extended the study to a sandwich structure containing spring-mass resonators. Chen et al. confirmed that waves were unable to propagate through the sandwich structure with the presence of a band gap, and thus concluded that such resonators could be used as mechanisms for suppressing flexural motion in a sandwich beam. Chen et al. also studied the wave attenuation and power flow characteristics of sandwich beams with different absorbers to reveal the energy dissipation [21].

Metamaterial plates are more common structures than beams in engineering applications. Examples of such applications are reduction of vibration during submarine activities and absorption of noise in residential houses. The difficulty lies in designing and analysing a metamaterial plate owing to its higher dimensions than those of metamaterial beams and bars. NOUH et al. [22, 23] investigated wave propagation through a metamaterial beam with periodic local resonances and extended the analysis to a metamaterial plate. The local resonance was achieved by cavities filled with a viscoelastic membrane that supported a small mass. Their results showed that within the band gaps, the metamaterial beam and plate could effectively attenuate and filter structural vibrations in the low-frequency range. The problem, however, was that although band gaps were obtained, the strength of both beam and plate was significantly reduced. GUSEV and WRIGHT [24] improved the work of NOUH et al. [16] by attaching spring-mass structures to a plate with different patterns, generating a band gap with double negativity. That work opened a way for flexural wave control. XIAO et al. [25] applied a plane wave expansion method to studying the propagation of flexural waves in a plate with spring-mass resonators. They found that resonance-type and Bragg-type band gaps coexisted in the plate, indicating a potential for vibration isolator design. PAI and his colleagues [26–28] theoretically and numerically analysed longitudinal and flexural wave propagation in metamaterial beams and flexural wave suppression in metamaterial plates via the Hamilton principle and

finite element (FE) simulation. Their numerical results for a sandwich metamaterial plate and a metamaterial plate with two resonators attached in series on one side showed that multiple band gaps were obtained for wave suppression. In the FE simulation, damping from the resonators was added, and the effects of damping on the band gaps and wave propagation were numerically investigated.

Damping exists in all practical engineering applications, and can greatly affect the performance of metamaterials. From the foregoing review, however, it is evident that most previous work has neglected the effects of damping from the host material (beams or plates) and resonators on the band gaps and wave propagation. Even in PENG and PAI's study [28], analysis of damping was performed by the FE simulation only, and the damping effect of the beam or plate material was also neglected. The working mechanism and effect of the damping from host material and resonators have rarely been theoretically presented and discussed. Moreover, it remains interesting if the series resonators are divided on both sides of the homogeneous plate. Does that produce wider and lower band gaps? To find the answers and provide better choices for the design of devices with multi-band gaps, we propose a new metamaterial with parallel resonators attached to a damped homogeneous plate with the aim of obtaining multiple resonance-type band gaps for flexural wave absorption and determining the effects of damping from the resonators on the wave propagation. The thin plate theory and Bloch's theorem are used here to derive the explicit formulations for the dispersion surfaces and the effective area mass density with damping considered. In this work, hysteretic damping from the plate material and resonators is first introduced for the theoretical analysis, and the damping effects on the band gaps and flexural wave propagation are systematically investigated. FE simulation and frequency response analysis (FRA) are performed to validate the theoretical results and to analyse the damping effect on wave propagation. Some practical models are proposed for future engineering implementations of the metamaterial.

## 2. Theoretical formulation

### 2.1. Dispersion surfaces and effective area mass density of the metamaterial plate

For a flexural wave with wave length$\lambda$, the distribution of normal force arising from the distribution of resonant elements is well approximated as continuous, provided that the distances among the adjacent elements on the plate surface are significantly smaller than the wavelength. As shown in Figs. 1 and 2, the acoustic metamaterial plate is composed of a homogeneous plate with Young's modulus $E$, Poisson's ratio $\nu$ and density $\rho$, and parallel attached resonators with the mass and stiffness $m_1$, $m_2$, $k_1$ and $k_2$, respectively. The size of a single metamaterial plate unit is $ax \times ay$. The resonators vibrate freely in the $z$direction.
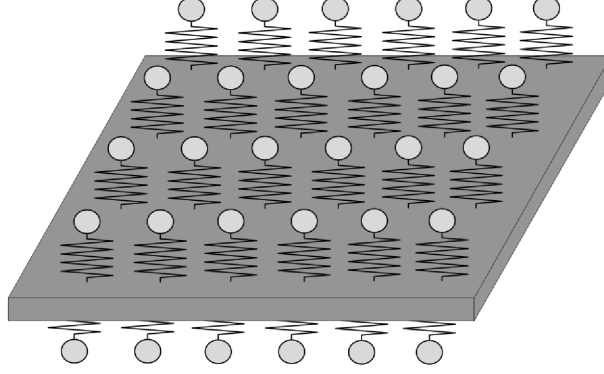
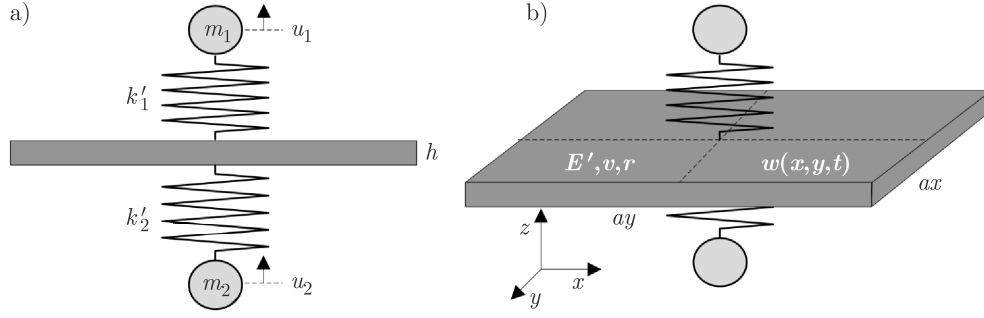FIG. 1. Acoustic metamaterial plate with parallel attached resonators arranged.



FIG. 2. Unit cell of the acoustic metamaterial: a) front view, b) perspective view.

Making use of the well-known Kirchhoff plate theory of the plate [29, 30] and Newton's second law, when a harmonic flexural wave is incident, the equations of the motion for a unit cell can be expressed as [31, 32]

$$(2.1) \qquad \rho h \frac{\partial^2 w(x,y,t)}{\partial t^2} =$$
$$-D \left( \frac{\partial^4 w(x,y,t)}{\partial x^4} + 2 \frac{\partial^4 w(x,y,t)}{\partial y^2 \partial x^2} + \frac{\partial^4 w(x,y,t)}{\partial y^4} \right) + q(x,y,t),$$

$$(2.2) \qquad q(0,0,t) = -nk_1(w_0(t) - u_1) - nk_2(w_0(t) - u_2),$$

$$(2.3) \qquad m_1 \ddot{u}_1 = k_1(w_0(t) - u_1),$$

$$(2.4) \qquad m_2 \ddot{u}_2 = k_2(w_0(t) - u_2),$$

where $w(x,y,t)$, $u_1$ and $u_2$ are the displacement of the plate deflection and vertical displacement of resonators, respectively. $n = 1/(ax \times ay)$ is the total number of dual resonators per unit area, and $D = Eh^3/[12(1 - \nu^2)]$ is the flexural rigidity of the plate.

For unit cells periodically placed in the $x, y$ direction, Bloch's theorem is adopted here to represent the displacement in the three equations above, and the wave solution in an infinite lattice is assumed to be in harmonic form as

$$(2.5) \quad w(x, y, t) = We^{i(\alpha x + \beta y + \omega t)} = w_0 e^{i(\alpha x + \beta y)}, \quad u_1 = U_1 e^{i\omega t}, \quad u_2 = U_2 e^{i\omega t}$$

with $\tilde{K}$ being the wavenumber, $\alpha$ and $\beta$ being its projections along the $x$, $y$ directions respectively, and $\tilde{K}^2 = \alpha^2 + \beta^2$. $W$, $U_1$ and $U_2$ are the complex-valued amplitudes of plate deflection and vertical displacement of resonators, respectively. When damping is taken into account, the complex Young's modulus and complex stiffness will be introduced with $E' = E(1 + j\eta_0)$, $k'_1 = k_1(1 + j\eta_1)$ and $k'_2 = k_2(1 + j\eta_2)$ in the frequency domain, where $\eta_0$ denotes the loss factor of the plate material, and $\eta_1$ and $\eta_2$ denote the loss factors of the springs. Substitution of Eq. (2.5) into Eqs. (2.1)–(2.4) yields

$(2.6)$

$$\begin{bmatrix} \rho h \omega^2 - D' \left( \alpha^2 + \beta^2 \right)^2 - nk'_1 - nk'_2 & nk'_1 & nk'_2 \\ k'_1 & m_1 \omega^2 - k'_1 & 0 \\ k'_2 & 0 & m_2 \omega^2 - k'_2 \end{bmatrix} \begin{Bmatrix} W \\ U_1 \\ U_2 \end{Bmatrix} = 0.$$

To obtain a nontrivial solution of $[W \ U_1 \ U_2]^{\mathrm{T}}$, the determinant of the coefficient matrix is set to zero, and its expanded equation is written as

$$(2.7) \qquad\qquad \gamma_1 \omega^6 + \gamma_2 \omega^4 + \gamma_3 \omega^2 + \gamma_4 = 0$$

with

$(2.8) \qquad \gamma_1 = \rho h m_1 m_2,$

$(2.9) \qquad \gamma_2 = \rho h(-m_1 k'_2 - m_2 k'_1) + m_1 m_2 [-D'(\alpha^2 + \beta^2)^2 - n(k'_1 + k')],$

$(2.10) \qquad \gamma_3 = \rho h k'_1 k'_2 + [-D'(\alpha^2 + \beta^2)^2 - n(k'_1 + k')](-m_1 k'_2 - m_2 k'_1)$
$\qquad\qquad - nk'^2_1 m_2 - nk'^2_2 m_1,$

$(2.11) \qquad \gamma_4 = [-D'(\alpha^2 + \beta^2)^2 - n(k'_1 + k')]k'_1 k'_2 + nk'^2_1 k'_2 - nk'^2_2 k'_1.$

For a specific wave vector $\mathbf{K} = (\alpha, \beta)$, there are six different angular frequencies. These angular frequencies, denoted as $\omega(\mathbf{K})$, are used to calculate the dispersion relation. Also, it is obvious that the angular frequencies are complex, and the dispersion relation can be obtained from them. The determinant of the matrix can also be translated as

$$(2.12) \qquad \alpha^2 + \beta^2 = \pm \frac{\omega}{\sqrt{D'}} \sqrt{\rho h + \frac{nk'_1 m_1}{k'_1 - m_1 \omega^2} + \frac{nk'_2 m_2}{k'_2 - m_2 \omega^2}}$$

for the analysis of wave attenuation, and the effective area mass density is

$$(2.13) \qquad\qquad \rho_{eff} = \rho + \frac{1}{h} \left( \frac{nk'_1 m_1}{k'_1 - m_1 \omega^2} + \frac{nk'_2 m_2}{k'_2 - m_2 \omega^2} \right).$$

Equation (2.12) presents the dispersion relation of the metamaterial plate, and Eq. (2.13) is the effective area mass density. From the dispersion relation, the band gaps can be obtained, and when the second item of Eq. (2.12) becomes zero, the effective area mass density equals the density of the homogeneous plate. When the second item becomes negative, with its absolute value greater than the value of $\rho$, the effective area mass density of the metamaterial plate also becomes negative. From Eq. (2.13), the interval of the negative mass density can be obtained by setting the right-hand side of Eq. (2.13) to zero and letting the denominator of Eq. (2.13) approach zero. Since the effective area mass density is determined from the corresponding dispersion relation (Eq. (2.12)), it can be concluded that the negative mass density ranges coincide with the band gaps.

We now focus on Eqs. (2.1) and (2.2). The force $q$ in Eq. (2.2) is the total force in the $z$ direction. A metamaterial plate with one vertical resonator attached to a unit cell can generate one band gap only. In this work, the unit cell of the metamaterial plate has two different resonators directly attached to the plate and can generate two band gaps. Assuming there are $n$ resonators attached to the unit cell of a homogeneous plate, it can form an n-band-gap-generating metamaterial plate. The positions of the attached resonators are unimportant if the total vertical force remains the same. This assumption can be easily validated by analysing the $n+1$ DOF system. However, in accordance with the concept of [33], more band gaps require more series of resonators. In the case of a metamaterial plate with multiple resonators arranged in series, the effect of the second- and higher-order resonators will be deactivated, resulting in more complex lower edges of band gaps, and less flexible tuning for the band gaps. If we compare these two metamaterials, the parallel attached metamaterial plate is superior in terms of practical application.

**2.2. Comparison with metamaterial plate series of attached dual resonators**

The parallel arrangement of resonators improves the performance of acoustic metamaterials with resonators attached in series. The advantages are identified in this subsection. Set $k_1/k_2 = \mu$, $m_1/m_2 = \theta$, $\omega_1 = \sqrt{k_1/m_1}$, $\omega_2 = \sqrt{k_2/m_2}$ and $\omega_2 < \omega_1$. The explicit formulas of the band gaps are too complex to show, but to facilitate the analysis, the lower edges of the first two band gaps for the plate proposed in this article are given as $[\omega_1, \omega_2]$. Using the same parameter setting and analysis method, the lower edges for the metamaterial in [30] are $\left[\sqrt{\left((\omega_1^2 + \omega_2^2 + \omega_1^2/\mu) \pm \sqrt{(\omega_1^2 + \omega_2^2 + \omega_1^2/\mu)^2 - 4\omega_1^2\omega_2^2}\right)\Big/2}\right]$. Comparing these lower edges, it can be seen that the lower edge of the first band gap for the metamaterial studied in this article is a little higher than that reported in [33],

while the lower edge of the second band gap is much lower than that in [33]. It is also noted that a change in either of the two resonators has no influence on the lower edges of the band gaps for the metamaterial considered in this work, which is different from the plate in [33].

To visually highlight the superiority of the characteristics of the metamaterial studied in this paper a comparison of the dispersive surfaces is shown in Figs. 3 and 4, with the parameters shown in Table 1. In the meantime, damping is neglected in this part.
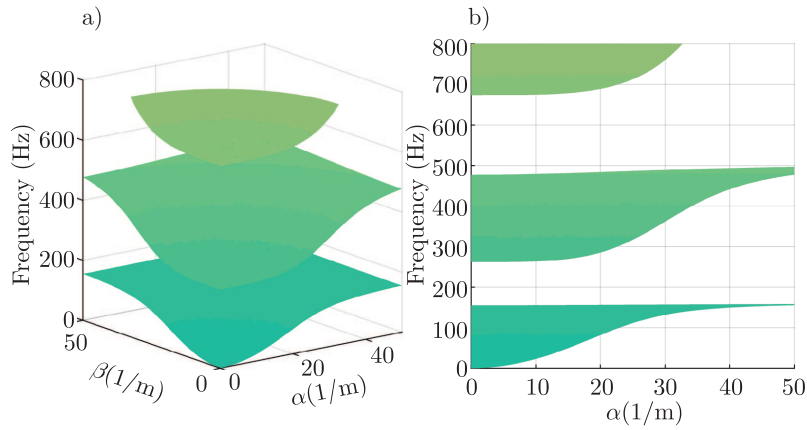


FIG. 3. Dispersion surface of the metamaterial plate with parallel attached resonators: a) perspective view, b) front view.
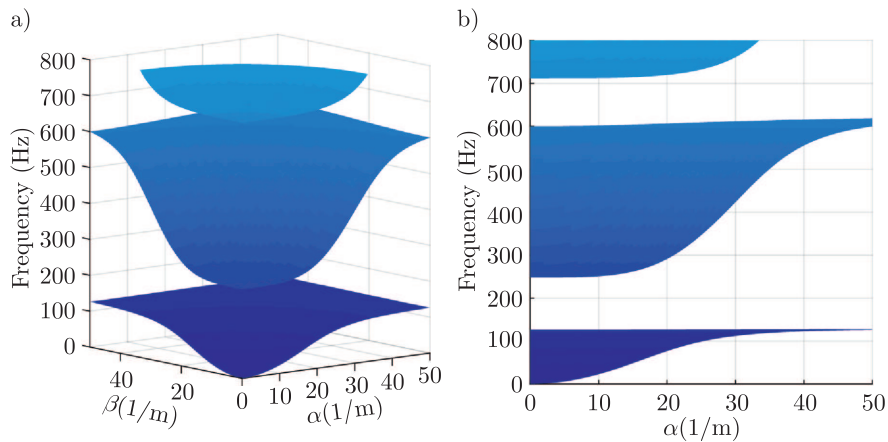


FIG. 4. Dispersion surfaces of the metamaterial plate with unilaterally attached resonators: a) perspective view, b) front view.

**Table 1.  Material properties of a single unit cell of the metamaterial plate.**

| Host plate | | Attached resonators | |
|---|---|---|---|
| Thickness | $h = 0.002$ m | Mass1 | $m_1 = 0.001$ kg |
| Density | $\rho = 7800$ kg/m$^3$ | Mass2 | $m_2 = 0.005$ kg |
| Poisson's ratio | $\nu = 0.3$ | Stiffness1 | $k_1 = 1 \times 10^4$ N/m |
| Young's modulus | $E = 2.1 \times 10^{11}$ Pa | Stiffness2 | $k_2 = 0.5 \times 10^4$ N/m |

A comparison of the dispersion surfaces of these two different metamaterial plates shows two main advantages of the metamaterial plate proposed in this paper over the metamaterial plate with unilaterally attached resonators. They are: (1) band gaps of the proposed metamaterial are 159.23 Hz $\sim$ 261 Hz and 503.54 Hz $\sim$ 674 Hz with the gap widths of 102 Hz and 171 Hz, respectively, whereas band gaps of the metamaterial plate with unilaterally attached dual resonators are 128 Hz $\sim$ 222 Hz and 623.88 Hz $\sim$ 711 Hz with the gap widths of 94 Hz and 87 Hz, respectively. It can be seen that the second band gap has been significantly widened, while the first band gap is nearly identical, (2) with the attached resonators arranged in parallel, the two band gaps are closer to each other, which means that it is easier to combine these two band gaps into a single broader one. From the theoretical analysis, changing the parameters of either of the parallel attached resonators has no effect on the lower bound of the other band gap, and (3) both structures generate two band gaps because of the resonance of the attached resonators, but the locations and the gap widths are significantly different. For the metamaterial with unilateral series of attached resonators, the interaction of the resonators connected in series changes the original resonance, slightly lowering the first band gap and dramatically pushing the second band gap to higher frequency range. As a result, the formation mechanism of band gaps becomes complicated, and it is difficult to adjust the attached resonators to achieve desired band gaps. The proposed metamaterial plate, on the other hand, retains the characteristics of the attached resonators because the separation of the two resonators largely isolates their influences on the resonances, even the band gaps, which means that each of the band gaps can be tuned individually.

### 2.3. Effect of damping on band gap and wave propagation

In the theoretical derivation, damping of the plate material and resonators is considered in the frequency domain. Subsection 2.2, however, was focused on showing the metamaterial's capability of generating complete band gaps, and therefore damping was ignored. In general, damping is always a significant factor in practical engineering. Therefore, the effects of damping on band gaps, especially on flexural wave propagation, are examined in this subsection. Addi-

tionally, the subsection explores whether the formation mechanism of the band gaps is attributable to the resonance or the Bragg scattering. The damping factor is the only variable, while the other parameters used in Table 1 are fixed during the calculation.

Figures 5 and 6 are the results obtained from Eq. (2.12), given a specific frequency. They show the effects of damping from the resonators and plate material, respectively.
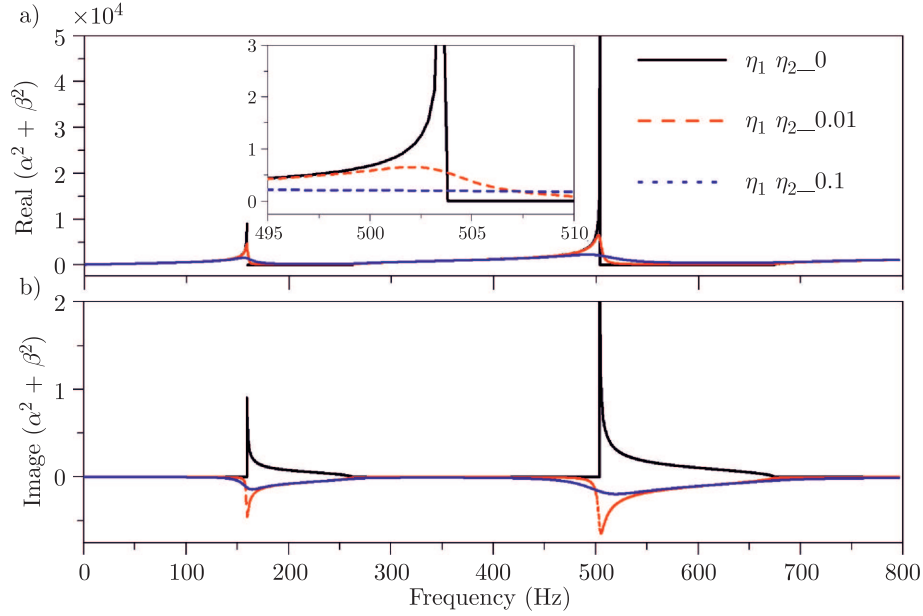


FIG. 5.  Effect of damping from the resonators on band gaps.

Figure 5 shows the effects of various damping values from the resonators on the band gaps with the damping of plate material equal to zero, $\eta_0 = 0$. First, when damping is set at zero, there are no real wavenumbers within the band gaps. Correspondingly, the imaginary part of the wavenumbers approaches infinity at two resonant frequencies of the parallel attached resonators, and decreases as the frequency increases. Let us set the wave vector as $K = (\alpha, \beta)$. Within the band gaps with damping equal to zero, we have

$$(2.14) \qquad |\mathbf{K}|^2 = |\alpha^2 + \beta^2| = \text{imaginary part.}$$

Therefore,

$$(2.15) \qquad \alpha = \kappa_{11} + j\kappa_{12}, \qquad \beta = \kappa_{21} + j\kappa_{22},$$

$$(2.16) \qquad w(x,y) = We^{-\kappa_{12}x - \kappa_{22}y}e^{j(\kappa_{11}x + \kappa_{21}y)}.$$

Equation (2.16) shows an evanescent wave field as the exponential function of distance along the $x, y$ direction.

When damping from the resonators is added, $\eta_1 = 0.01$ and $\eta_2 = 0.01$, the value of the imaginary part of the wavenumber decreases, and the real part is no longer zero but some small value which can be expressed as

$$(2.17) \qquad |\mathbf{K}|^2 = |\alpha^2 + \beta^2| = \text{real part} + \text{imaginary part}.$$

Therefore,

$$(2.18) \qquad \alpha = \kappa_{11} + j\kappa_{12}, \qquad \beta = \kappa_{21} + j\kappa_{22},$$

$$(2.19) \qquad w(x,y) = We^{-\kappa_{12}x - \kappa_{22}y}e^{j(\kappa_{11}x + \kappa_{21}y)}.$$

Since $|\kappa_{12}| > |\kappa_{11}|$ and $|\kappa_{22}| > |\kappa_{21}|$, the amplitudes of the flexural wave decrease as it propagates through the metamaterial, while the attenuation rate slows. Furthermore, with a resonator damping increasing to $\eta_1 = 0.1$ and $\eta_2 = 0.1$, the absolute value of the imaginary part of the wave vector becomes no greater than that of the real part for the band gaps and frequency ranges beside the band gaps. In this case, the response of the plate is decreased and smoothed, while the band gap effect is deactivated.

Figure 6 reveals the effects of the damping of the plate on the band gaps with damping of resonators equal to zero, $\eta_1 = 0$ and $\eta_2 = 0$. As the damping of the metamaterial increases, within the band gaps, the real part of the wavenum-
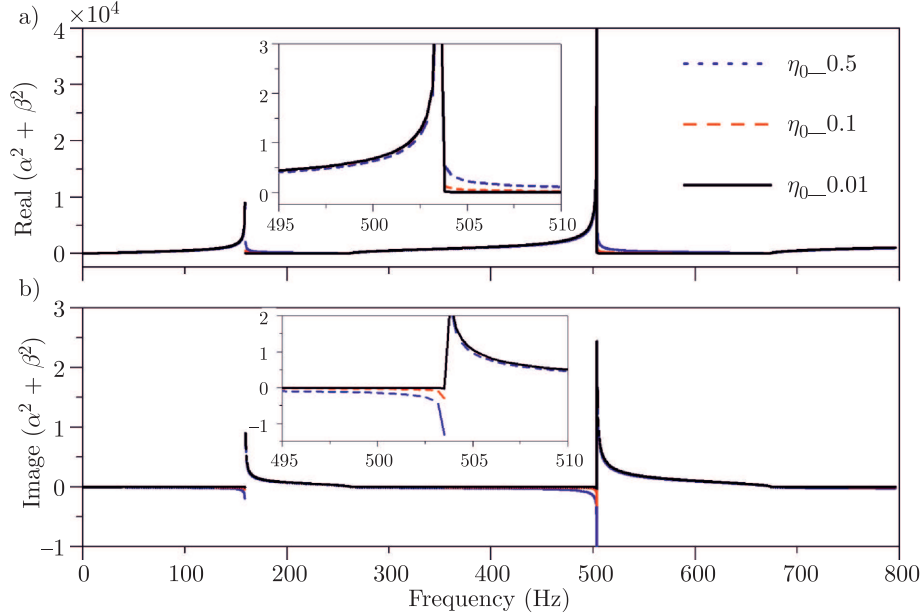


FIG. 6. Effect of damping from the plate on band gaps.

ber increases while the imaginary part is slightly smaller. This means that the attenuation capability is deactivated little, while the waves oscillate simultaneously. In Fig. 6b, for the edges of band gaps, the wavenumbers' imaginary part becomes much greater than the previous values and large attenuation occurs correspondingly, leading to broad band gaps. Simultaneously, outside the band gaps, the imaginary part of the wavenumber is not always zero, especially for the edges of band gaps, which means that attenuation within these frequency ranges occurs and responses are lowered and smoothed. At the resonance frequencies, i.e., 159 Hz and 503 Hz, there are two steps when the damping is at $\eta_0 = 0.5$. These two steps are caused by the vigorous resonance of the two resonators.

In summary, damping from the plate and resonators has a more significant influence on the band gaps and wave propagation. These effects help to widen the band gaps and smooth and lower the frequency response of the plate. Too much damping, whether from the plate or the resonators, can deactivate the effect of band gaps.

### 2.4. The effective area mass density with various damping values

In Subsection 2.1, the explicit formula Eq. (2.13) of the effective mass density was derived. To analyse the characteristics of the effective mass density with various damping values, the effective density vs. frequency is plotted in Fig. 7. In the calculation, the parameters are the same as those in Subsection 2.3 with various values of damping.
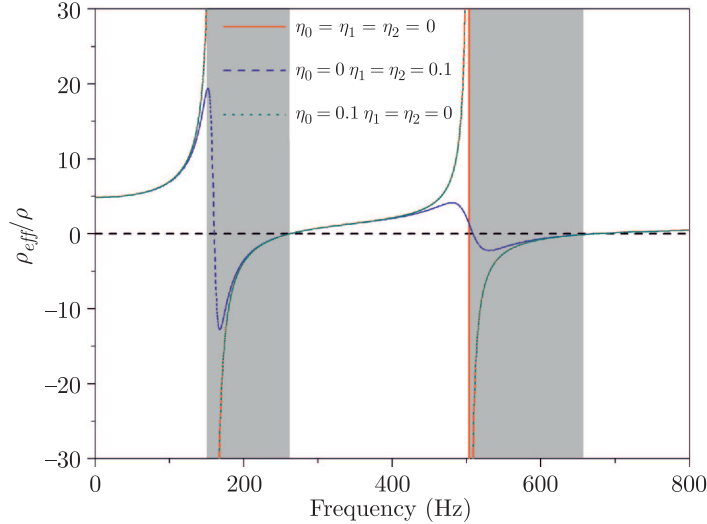


FIG. 7. The effective area mass density of the metamaterial with different damping values.

In Fig. 7, there are three curves for effective mass density with different damping factors. However, the effective density curve without damping coincides with that of non-plate damping, which means that the plate damping has little influence on the effective mass density. Actually, from Eq. (2.13) it can be found that the effective mass density has nothing to do with plate rigidity, not to mention plate material damping. The non-damping density curve reaches unbounded positive values at the resonance frequencies of the two attached resonators, then drops to negative infinity and remains negative within the band gaps, while in the other bands it is positive. The steps at the resonance frequency are attributable to the instantaneous energy transformation and storing of the resonators which vibrate vigorously and generate large inertia forces to counterbalance the bending force of the plate. When damping is added to the resonators (referring to the blue dashed line in Fig. 7), the value of the density at resonance frequencies is greatly decreased, because the resonance energy is damped out. It should be noted that the starting frequencies of the negative-density range are enhanced, corresponding to the shaded areas which are decreased. As a result, damping from the resonators may reduce the singularity of the mass density, with the sacrifice of shrinking of negative-density ranges.

The negative mass density provides an explanation for the occurrence of the band gaps from a specific perspective. As in the previous assumption, in the low-frequency range, because the wave length is much longer than the reciprocal lattice constant, the metamaterial can be treated as a homogeneous plate with effective parameters. For the proposed metamaterial plate, using the effective area mass density, the closed form governing equation can be expressed as

$$(2.20) \quad \rho_{eff} h \frac{\partial^2 w(x,y,t)}{\partial t^2} - D\left( \frac{\partial^4 w(x,y,t)}{\partial x^4} + 2\frac{\partial^4 w(x,y,t)}{\partial y^2 \partial x^2} + \frac{\partial^4 w(x,y,t)}{\partial y^4} \right) = 0.$$

Substitution of the harmonic vibration $w(x,y,t) = We^{i(\omega t - \alpha x - \beta y)}$ into Eq. (2.20) yields

$$(2.21) \qquad\qquad (\nabla^2 \nabla^2 - (\alpha^2 + \beta^2)^2)W = 0,$$

$$(2.22) \qquad\qquad \alpha^2 + \beta^2 = \frac{\omega}{\sqrt{D}}\sqrt{2h\rho_{eff}}.$$

From Eq. (2.22), it can be seen that, when the effective mass density is negative, it will lead to complex wave vectors. Assuming $\alpha = \kappa_{11} + j\kappa_{12}$ and $\beta = \kappa_{21} + j\kappa_{22}$ with $\kappa_{11}, \kappa_{21} > 0$ and real, the flexural vibration can be expressed as

$$(2.23) \qquad\qquad w(x,y,t) = We^{-\kappa_{11}x - \kappa_{21}y}e^{i(\kappa_{12}x + \kappa_{22}y + \omega t)}.$$

Equation (2.23) indicates that within the negative-density ranges, the amplitude of the flexural wave is evanescent, and attenuates exponentially along the

$x, y$ directions. When damping of the resonators is added, the absolute value of the effective density decreases. This may result in less attenuation within the negative-density ranges, as well as the band gaps.

## 3. FE simulation with ANSYS

The FE simulation is conducted here to validate the theoretical results of the damping effects on the band gaps and wave propagation performance of the proposed metamaterial. The fundamentals of FE methods can be found in the literature [34–37]. Details of the FE modelling with ANSYS 15.0 are described here with the material properties used in Table 1.

Masses are modelled using element MASS 21 with free vibration in the $z$ direction. Springs are modelled using element COMBIN 14 in the $z$ direction. The homogeneous plate is modelled by using element SHELL 63. The meshing size is 0.005 m, and the type of meshing is mapped to ensure accuracy.

Figure 8 shows the FE model composed of three parts. The first and third parts are the homogeneous plate with $50 \times 80$ unit cells respectively; in the middle part, $200 \times 80$ unit cells lie along the $x$-$y$ plane. The FRA is used to obtain the steady response of the metamaterial plate under a harmonic excitation with a free-boundary condition. The harmonic excitation $F = F_0 e^{j\omega t}$, $F_0 = 100N$ is applied on the central node of the left line, as shown in Fig. 8.
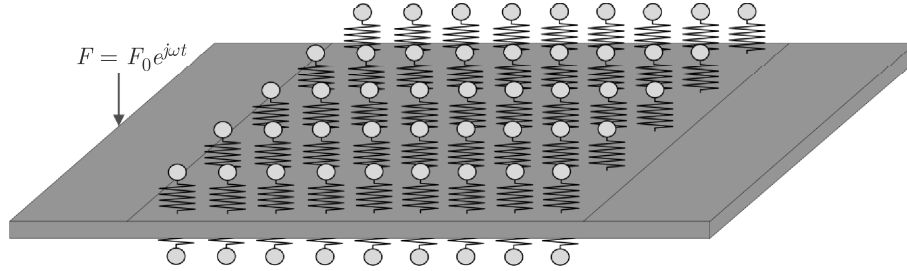


Fig. 8. Schematic FE model of the metamaterial plate with parallel attached resonators.

### 3.1. Effect of the damping on band gaps

Since the simulation attempts to capture the vibration of the plate in engineering applications, damping is an important factor to be considered. From previous theoretical analysis, we are aware that damping has a significant influence on the band gaps as well as on wave propagation. By using the relation between the viscous damping and the damping factor $c_1 = 2\eta_1\sqrt{k_1 m_1}$, $c_2 = 2\eta_2\sqrt{k_2 m_2}$, viscous damping of the resonators is added on the springs of the finite element model. For the plate, damping $\eta_0 = 0.1$ is involved through the material prop-

erties (i.e., in the complex Young's modulus). There are four sets of parameters
to feature the effects of damping:

(1) $\eta_1 = 0$, $\eta_2 = 0$, $\eta_0 = 0$,
(2) $\eta_1 = 0.01$, $\eta_2 = 0.01$, $\eta_0 = 0$,
(3) $\eta_1 = 0.1$, $\eta_2 = 0.1$, $\eta_0 = 0$,
(4) $\eta_1 = 0$, $\eta_2 = 0$, $\eta_0 = 0.1$.

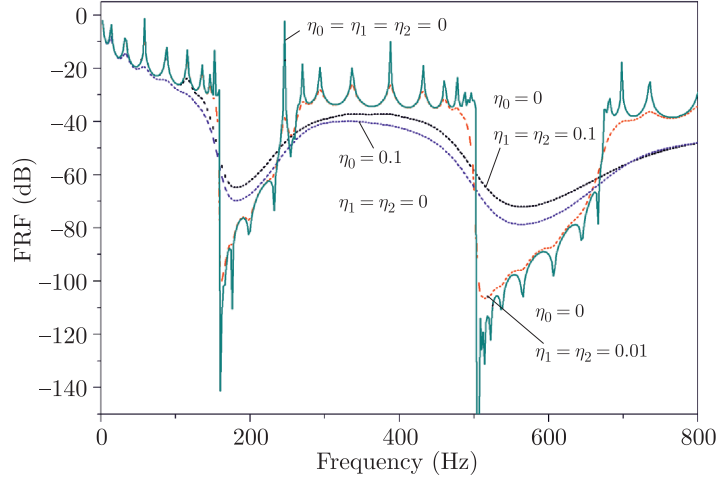The corresponding frequency response function (FRF) is shown in Fig. 9.



Fig. 9. FRF of nodes at $x = 3$ m with different parameter settings.

In Fig. 9, four lines in different colours represent the FRF under different pa-
rameter settings. Firstly, considering the solid line with $\eta_1 = 0$, $\eta_2 = 0$, $\eta_0 = 0$,
two large dips are evident in which the flexural waves are greatly attenuated.
These two dips coincide with the band gaps described in the theoretical analy-
sis. The attenuation within the band gaps decreases as the frequency increases,
because the resonance occurs at the lower edges of the two band gaps, and the
resonators vibrate vigorously. With an increase in frequency, the resonances die
down and the stored energy drops, as does the influence on wave propagation.
The numerical results indicate that the metamaterial can restrain wave propa-
gation in two specific frequency ranges; on the other hand, the numerical results
validate the accuracy of the theoretical derivation. Secondly, from a comparison
of the solid line with the dashed line, which represent the metamaterial without
damping ($\eta_1 = 0$, $\eta_2 = 0$, $\eta_0 = 0$) and with minor damping from the resonators
($\eta_1 = 0.01$, $\eta_2 = 0.01$, $\eta_0 = 0$), respectively, it is evident that the band gap
effect remains, while the response peaks are slightly decreased from the first
band gap to the higher frequency range (the response in the lower frequency
range changes little). With damping from the resonators increasing to $\eta_1 = 0.1$,

$\eta_2 = 0.1$, $\eta_0 = 0$, corresponding to the dotted line in Fig. 9, both band gaps are widened, while the band gap effect is dramatically deactivated. For the middle and higher frequency ranges, responses are greatly lowered and smoothed, and the entire energy of the system is reduced, effects of which are attributed to the damping out of energy. However, the response changes little from $0 \sim 150$ Hz. This drawback can be remedied by the damping from the host material, shown as the dash-dotted line ($\eta_1 = 0$, $\eta_2 = 0$, $\eta_0 = 0.1$). Damping from the plate can lower the response across the whole frequency range, especially for ranges of $0 \sim 150$ Hz and 260 Hz $\sim 503$ Hz. Comparison of the curves of $\eta_1 = 0.1$, $\eta_2 = 0.1$, $\eta_1 = 0$ and $\eta_1 = 0$, $\eta_2 = 0$, $\eta_0 = 0.1$ reveals that damping from the host material has less influence on the band gap effect and improves the whole performance of the metamaterial plate.

In real engineering applications, damping cannot be neglected. How to utilise damping to acquire desired outcomes needs investigation. Thus, this paper can provide guidance for practical implementation of the metamaterial plate for the absorption of multi-frequency flexural elastic wave and the suppression of structural vibration.

### 3.2. Vibration modes for wave propagation

To observe the wave propagation within the band gaps and the pass band graphically, the vibration modes are investigated and some results are presented in Fig. 10. Figure 10a shows the wave propagation under 200 Hz, which is within the first band gap, Fig. 10b displays the mode shape under 400 Hz, which is in the pass band, and Fig. 10c shows the wave propagation under 600 Hz, which is within the second band gap.

In Fig. 10a it can be seen that the plate in the first part vibrates vigorously as the excitation begins, but when the waves reach the middle section (the metamaterial part), they attenuate dramatically. Because the vibration has been blocked as it approaches the metamaterial, the rest of the metamaterial and the third part remain quiet. From the analysis of the vibration behaviour, we find that it is the downside resonator that vibrates vigorously to generate an inertial force to counterbalance the shear forces of the plate, and consequently the waves cannot pass through. In striking contrast to Fig. 10a, vibration in the third part in Fig. 10b is similar to that in the first part, which means the waves pass through the plates without attenuation. Figure 10c is much like Fig. 10a regarding the wave packets. Waves with a frequency of 600 Hz are blocked because of the upside resonator vibration. With the attenuation mechanism, i.e., the different resonances from the upside and downside, it can be seen that the band gap is formed because the parallel attached resonators vibrate vigorously and generate inertial forces to counterbalance the shear forces induced by the
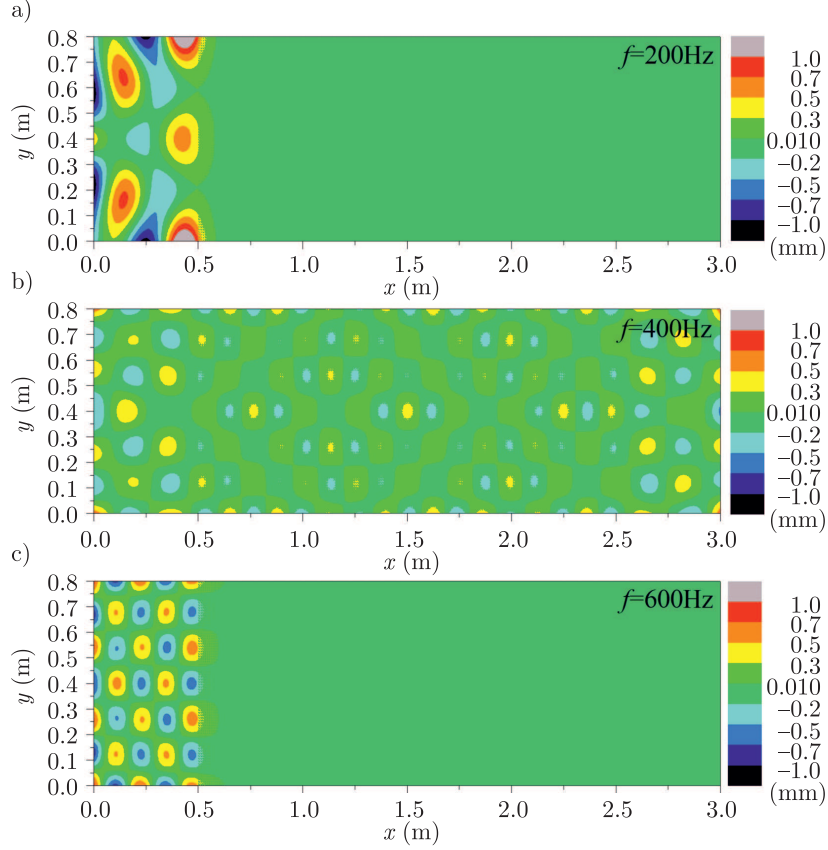
Fig. 10. Vibration modes under different frequencies without damping.

plate. Owing to the separation of the two resonators, the band gaps can be tuned flexibly with a little influence on each other, a result that is significant in the fields of low-frequency vibration and noise control.

### 3.3. Wave propagation history within the band gaps

Although it has been demonstrated that the proposed metamaterial plate can prevent wave propagation within the band gaps, the propagation of elastic waves in transient analysis is still essential for dynamic analysis. In the following simulation, damping is removed to promote deep understanding of the wave propagation through the structure. The plate is simply supported at four corner nodes. The excitation is at the central node on the left side line with $F_1 = \sin(2\pi(200 \text{ Hz})t)$, $F_2 = \sin(2\pi(600 \text{ Hz})t)$ and $F_3 = \sin(2\pi(200 \text{ Hz})t) + \sin(2\pi(600 \text{ Hz})t)$. The response is obtained from the nodes on the centreline of the metamaterial plate at different distances from the incident waves. The frequencies of the excitation are all located within the band gaps.
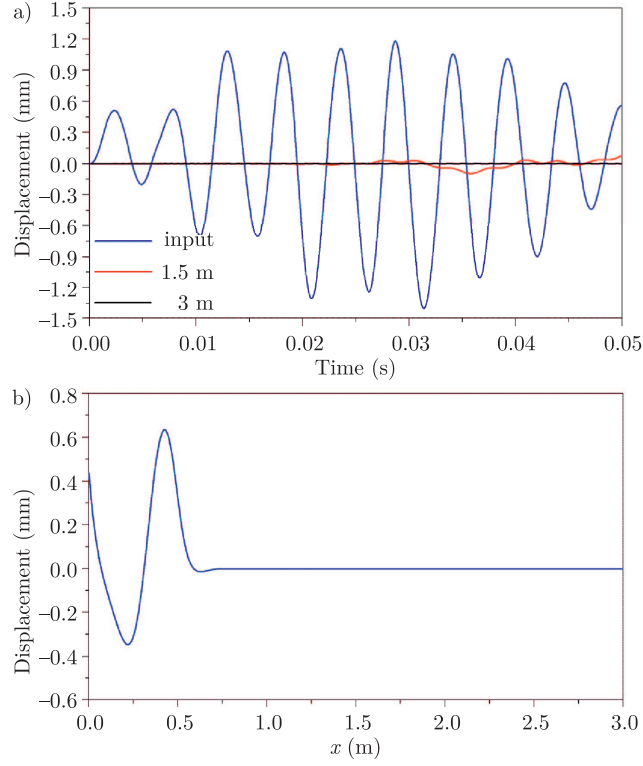
Fig. 11. Under $f$=200 Hz: a) transient analysis, b) vibration mode of the centreline from the FRA.

Figure 11a shows the transient vibrations of nodes on the centreline ($y = 0.4$ m) along the $x$ axis at $x = 0$ m, 1.5 m and 3 m, which lie on the three different parts of the plate. When the excitation begins at $x = 0$ m, the plate vibrates at the specific frequency of 200 Hz and reaches a steady state. It is obvious that, as the wave propagates through the metamaterial plate, the amplitude of the wave attenuates with the increase of distance as well as with the function of the metamaterial. When the wave reaches the node at $x = 1.5$ m, it takes about 0.002 s during which the wave speed can be calculated as 750 m/s. Figure 11b shows the mode shape on the centreline of the plate from the FRA. It can be seen that waves in the plate without attached resonators propagate with no attenuation. As the waves reach the metamaterial plate, the amplitude of the metamaterial plate decreases dramatically, indicating that the metamaterial blocks the waves efficiently. Since the boundary condition is simply supported at the two corner nodes on the right side, there are no reflected waves to interfere with the mode shape. Therefore, the metamaterial plate can efficiently prevent wave propagation within the first band gap.
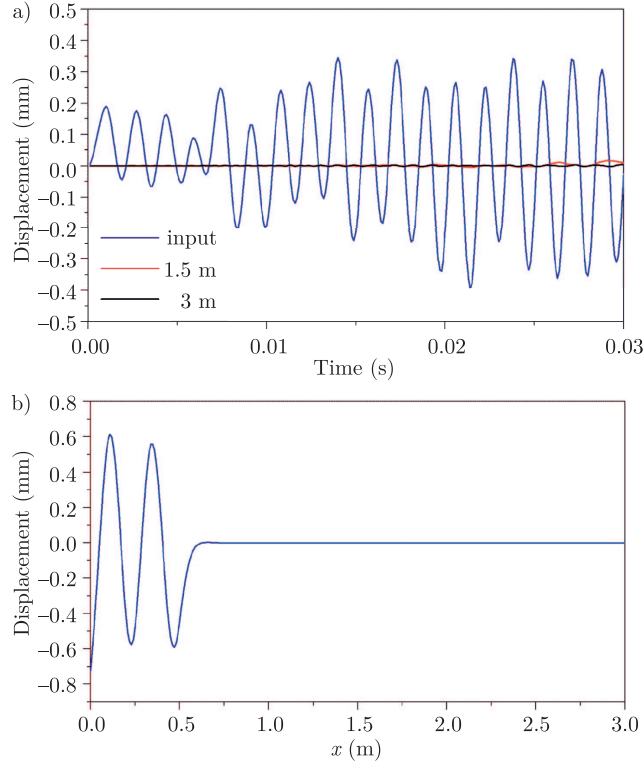
Fig. 12. Under $f = 600$ Hz: a) transient analysis, b) vibration mode of the centreline from the FRA.

In a manner similar to that in Fig. 11, Fig. 12a shows the wave propagation history progressing with the frequency of 600 Hz in transient analysis, and Fig. 12b shows the mode shapes of the metamaterial plate under the frequency of 600 Hz from the FRA. In Fig. 12a, it is obvious that it takes about 0.01 s for the plate to reach the steady state, and as the distance of the node from the excitation points increases, the wave amplitudes decrease. In Fig. 12b, the plate at $x > 0.75$ m has almost no vibration where the metamaterial plate starts at $x = 0.5$ m. The dramatic attenuation of the wave in the complex plate shows the capability of the metamaterial plate, which can be useful in a vibration isolator to restrain flexural wave propagation.

In engineering applications, waves always propagate with a combination of different frequencies, and it is therefore useful for a metamaterial to have the capacity to prevent multiple band flexural waves. In this simulation, the frequency of the excitation is a combination of 200 Hz and 600 Hz frequencies, which are within the first and second band gap, respectively. The transient result is presented in Fig. 13.
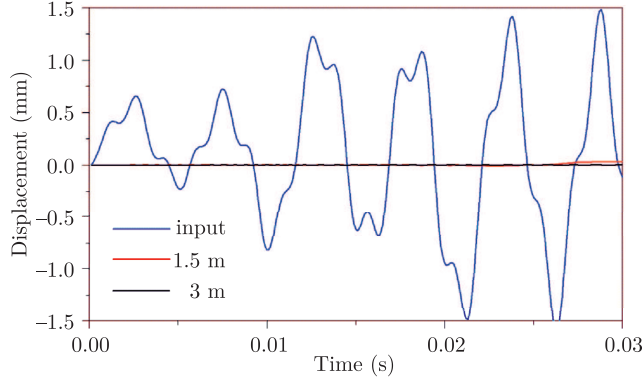
FIG. 13.  Transient analysis under $f = (200 \text{ Hz} + 600 \text{ Hz})$.

Figure 13 shows the elastic wave propagation history in the metamaterial plate. After the excitation begins, the plate reaches a steady state in 0.02 s. It can be seen that the wave attenuates quickly as it reaches the metamaterial plate. From the previous analysis, both the parallel attached resonators vibrate to generate the corresponding inertial force to counterbalance the shear forces from the plate to block the waves. It can be concluded that the metamaterial can restrain multi-frequency waves propagating simultaneously within the band gaps.

## 4. Discussion about the implementation of the metamaterial

This study has provided a conceptual design for harmonic suppression using damped metamaterial exhibiting negative effective mass density. Theoretical derivation and computer simulation validation were presented. A detailed analysis of the acoustic metamaterial with parallel attached resonators showed that the metamaterial proposed in this paper could efficiently block flexural waves within the band gaps. Although much work has been done to investigate elastic wave suppression through metamaterial, damping effects on the band gaps from the host material still remain systematically investigated. This article has provided full explanation of the damping arising from different constituents of the metamaterial, which is close to practical implementation. In this section, we present two different practical models based on this metamaterial unit, as shown in Fig. 14.

(1) In general, springs with viscous damping in the theoretical model can be realised using silicon rubber bars/beams, as shown in Fig. 14a. In this case, the effective stiffness of the rubber can be obtained by
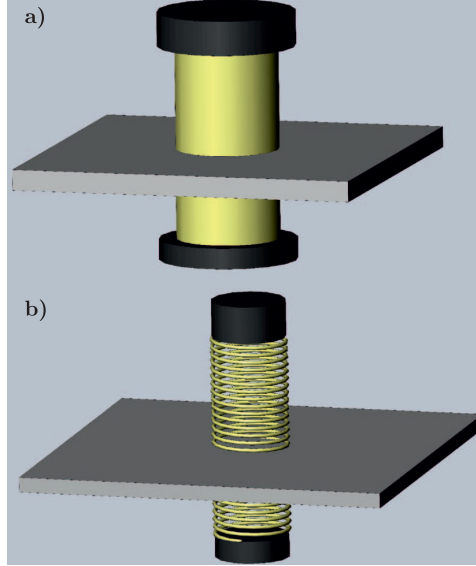
(4.1)
$$K' = \frac{E'S}{L},$$

Fig. 14. Practical model of the acoustic metamaterial plate with parallel attached resonators: a) silicon rubber bars/beams, and b) real steel springs with viscous damping (dashpot).

where $E'$, $S$ and $L$ are the complex Young's modulus, the cross-section and the length of the rubber, respectively, under the circumstance of a short rubber bar. Actually, there are several constitutive models for the rubber when it is used as a damping component, examples being the Flory–Erman model and the Arruda–Boyce eight-chain model. To build the practical metamaterial precisely, further investigation of the modelling of the rubber should be developed, which is merely introduced here. Hysteretic damping can also be obtained by the introduction of the damping coefficient of the rubber.

(2) Another possible configuration is real steel springs with viscous damping (dashpot). As shown in Fig. 14b, the spring-mass resonators are parallel, attached to the homogeneous plate. In this case, the mounting requirements need to be examined. Any slippage among contacts of the steel springs and the masses should be noted, as that can greatly influence the performance of the metamaterial. The central point of the mass should be consistent with that of the springs in cases of torsion and rotation. Such cases will be further analysed in a future study to provide more detailed guidance.

We are aware that the analysis in this work is limited: the host plate is assumed to be homogeneous elastic, the attached resonators ideally vibrate in the $z$ direction and theoretical and numerical analysis is limited to unconstrained systems, to name a few limitations. However, since a free-boundary system demonstrates a worst-case scenario, unconstrained systems can ideally satisfy

one's needs for a particular practical purpose with desirable properties under all circumstances. Moreover, viscoelastic material behaviour is neglected. Instead, hysteretic damping of the resonators and host plate is analysed numerically for the practical engineering. Furthermore, when the proposed configuration is used in practical engineering, the coupling loss factor may be another quantity influencing the behaviour of the metamaterial plate. The attached resonators and the host plate are independent constituents. When they are assembled together for vibration suppression, power flow among these constituents determines the vibration modes. The coupling loss factor and power flow can be analysed using statistical energy methods, which will be elaborated in future work.

For the practical model proposed in this part, the connection between the resonators and the plate is no longer a single point. Consequently, the results may differ from the theoretical results, but the trends of the curves and conclusions show the capability of the metamaterial. These matters should be dealt with in future experimental validation.

Practical engineering may need to apply the concept of attaching damped resonators to a cylindrical shell in parallel configuration, such as a submarine shell, and it may be useful to construct a metamaterial cylinder shell for vibration absorption and wave attenuation. In our future analysis, the practical metamaterial plate model and theoretical metamaterial cylinder model will be developed. The analysis presented in this article may provide a foundation for future complex implementations. There is still much room in this work for exploration in practical engineering design.

## 5. Conclusion

The acoustic characteristics of a damped metamaterial plate composed of a homogeneous plate with parallel attached resonators were investigated theoretically and numerically. Comparison with a metamaterial plate with two resonators attached in series showed that the second band gap of the proposed metamaterial is much wider and lower, whereas the first band gap changes little. For the metamaterial plate with parallel attached resonators, the lower edges of the band gap isolate each other, facilitating merging of the band gaps into a wider single band gap and leading to better potential for practical application. Damping from different parts of the metamaterial unit was fully investigated with respect to the band gaps and wave propagation performance. The results reveal that damping from the host plate can broaden the band gaps, and smooth and lower the responses across the whole frequency range. At the same time, damping of the resonators can greatly affect the effective mass density within the negative-density ranges through vigorous resonance and damping out the energy. FE modelling and the FRA were adopted to investigate wave propagation

through the proposed metamaterial plate. The addition of a reasonable level of damping in the simulation efficiently lowered and smoothed the responses, a finding which was consistent with the theoretical results. On the other hand, a high level of damping of the resonators dramatically deactivated the band gap effect. Separation of the two resonators weakened the effects of damping from each other, facilitating detection of the source of damage caused by damping. The mode shapes with different frequencies showed the behaviour of the waves within and outside the band gaps. They also revealed that the metamaterial plate is based on the concept of conventional multi-frequency vibration absorbers which generate inertial forces to counteract the shear forces induced by the flexural waves within the band gaps.

**5.1. Acknowledgement**

## References

1. S.H. Lee, C.M. Park, Y.M. Seo, Z.G. Wang, C.K. Kim, *Acoustic metamaterial with negative density*, Physics Letters A, **373** (48), 4464–4469, 2009.

2. M. Oudich, B. Djafari-Rouhani, Y. Pennec, M.B. Assouar, B. Bonello, *Negative effective mass density of acoustic metamaterial plate decorated with low frequency resonant pillars*, Journal of Applied Physics, **116** (18), 184504, 2014.

3. T. Wang, H. Wang, M.P. Sheng, Q.H. Qin, *Complete low-frequency bandgap in a two-dimensional phononic crystal with spindle-shaped inclusions. Project supported by the China Scholarship Council*, Chinese Physics B, **25** (4), 046301, 2016.

4. S.H. Lee, C.M. Park, Y.M. Seo, Z.G. Wang, C.K. Kim, *Acoustic metamaterial with negative modulus*, Journal of Physics: Condensed Matter, **21** (17), 175704, 2009.

5. N. Fang, D. Xi, J. Xu, M. Ambati, W. Srituravanich, C. Sun, X. Zhang, *Ultrasonic metamaterials with negative modulus*, Nature Materials, **5**(6), 452–456, 2006.

6. T. Wang, M.-P. Sheng, Z.-W. Guo, Q.H. Qin, *Flexural wave suppression by an acoustic metamaterial plate*, Applied Acoustics, **114**, 118–124, 2016.

7. T. Brunet, A. Merlin, B. Mascaro, K. Zimny, J. Leng, O. Poncelet, C. Aristégui, O. Mondain-Monval, *Soft 3D acoustic metamaterial with negative index*, Nature Materials, **14** (4), 384–388, 2015.

8. H.H. Huang, C.T. Sun, G.L. Huang, *On the negative effective mass density in acoustic metamaterials*, International Journal of Engineering Science, **47** (4), 610–617, 2009.

9. G.L. Huang, C.T. Sun, *Band gaps in a multiresonator acoustic metamaterial*, Journal of Vibration and Acoustics, **132** (3), 031003–031003, 2010.

10. H.H. HUANG, C.T. SUN, *Theoretical investigation of the behavior of an acoustic meta-material with extreme Young's modulus*, Journal of the Mechanics and Physics of Solids, **59** (10), 2070–2081, 2011.

11. S.A. POPE, H. LAALEJ, S. DALEY, *Performance and stability analysis of active elastic metamaterials with a tunable double negative response*, Smart Materials and Structures, **21** (12), 125021, 2012.

12. X. WANG, *Dynamic behaviour of a metamaterial system with negative mass and modulus*, International Journal of Solids and Structures, **51** (7–8), 1534–1541, 2014.

13. X.N. LIU, G.K. HU, G.L. HUANG, C.T. SUN, *An elastic metamaterial with simultaneously negative mass density and bulk modulus*, Applied Physics Letters, **98** (25), 251907, 2011.

14. T. WANG, M.P. SHENG, Q.H. QIN, *Multi-flexural band gaps in an Euler–Bernoulli beam with lateral local resonators*, Physics Letters A, **380** (4), 525–529, 2016.

15. D. YU, Y. LIU, G. WANG, H. ZHAO, J. QIU, *Flexural vibration band gaps in Timoshenko beams with locally resonant structures*, Journal of Applied Physics, **100** (12), 124901, 2006.

16. Y. LIU, D. YU, L. LI, H. ZHAO, J. WEN, X. WEN, *Design guidelines for flexural wave attenuation of slender beams with local resonators*, Physics Letters A, **362** (5–6), 344–347, 2007.

17. D. YU, Y. LIU, G. WANG, L. CAI, J. QIU, *Low frequency torsional vibration gaps in the shaft with locally resonant structures*, Physics Letters A, **348** (3–6), 410–415, 2006.

18. J.S. CHEN, B. SHARMA, C.T. SUN, *Dynamic behaviour of sandwich structure containing spring-mass resonators*, Composite Structures, **93** (8), 2120–2125, 2011.

19. J.S. CHEN, C.T. SUN, *Wave propagation in sandwich structures with resonators and periodic cores*, Journal of Sandwich Structures and Materials, **15** (3), 359–374, 2013.

20. J.S. CHEN, C.T. SUN, *Dynamic behavior of a sandwich beam with internal resonators*, Journal of Sandwich Structures and Materials, **13** (4), 391–408, 2011.

21. J.S. CHEN, R.T. WANG, *Wave propagation and power flow analysis of sandwich structures with internal absorbers*, Journal of Vibration and Acoustics, **136** (4), 041003–041003, 2014.

22. M. NOUH, O. ALDRAIHEM, A. BAZ, *Vibration characteristics of metamaterial beams with periodic local resonances*, Journal of Vibration and Acoustics, **136** (6), 061012–061012, 2014.

23. M. NOUH, O. ALDRAIHEM, A. BAZ, *Wave propagation in metamaterial plates with periodic local resonances*, Journal of Sound and Vibration, **341** (0), 53–73, 2015.

24. V.E. GUSEV, O.B. WRIGHT, *Double-negative flexural acoustic metamaterial*, New Journal of Physics, **16** (12), 123053, 2014.

25. Y. XIAO, J. WEN, X. WEN, *Flexural wave band gaps in locally resonant thin plates with periodically attached spring–mass resonators*, Journal of Physics D: Applied Physics, **45** (19), 195401, 2012.

26. P.F. PAI, *Metamaterial-based broadband elastic wave absorber*, Journal of Intelligent Material Systems and Structures, **21** (5), 517–528, 2010.

27. H. SUN, X. DU, P.F. PAI, *Theory of metamaterial beams for broadband vibration absorption*, Journal of Intelligent Material Systems and Structures, **21** (11), 1085–1101, 2010.

28. H. Peng, P.F. Pai, *Acoustic metamaterial plates for elastic wave absorption and structural vibration suppression*, International Journal of Mechanical Sciences, **89** (0), 350–361, 2014.

29. Q.H. Qin, *The Trefftz Finite and Boundary Element Method*, WIT Press, Southampton 2000.

30. Q.H. Qin, *Trefftz finite element method and its applications*, Applied Mechanics Reviews, **58** (5), 316–337, 2005.

31. K.F. Graff, *Wave Motion in Elastic Solids*, Dover Publications, 1975.

32. Q.H. Qin, *Transient plate bending analysis by hybrid Trefftz element approach*, Communications in Numerical Methods in Engineering, **12** (10), 609–616, 1996.

33. H. Peng, P.F. Pai, H. Deng, *Acoustic multi-stopband metamaterial plates design for broadband elastic wave absorption and vibration suppression*, International Journal of Mechanical Sciences, **103**, 104–114, 2015.

34. G. Dhatt, E. Lefrançois, G. Touzot, *Finite Element Method*, John Wiley & Sons, 2012.

35. Q.H. Qin, H. Wang, *Matlab and C Programming for Trefftz Finite Element Methods*, CRC Press, New York, 2008.

36. Q.H. Qin, *Hybrid-Trefftz finite element method for Reissner plates on an elastic foundation*, Computer Methods in Applied Mechanics and Engineering, **122** (3–4), 379–392, 1995.

37. Q.H. Qin, *Solving anti-plane problems of piezoelectric materials by the Trefftz finite element approach*, Computational Mechanics, **31** (6), 461–468, 2003.